(BW = 3.19 MHz) which is close to the simulation results. The measured results show wider bandwidth due to the ohmic loss through the antenna structure.

Far–field pattern of the antenna has been simulated using HFSS@ (High Frequency Structure Synthesizer) and is plotted in Figure 6. Figure 6a shows *Gx* (gain in the *x* direction) which is considered copolarization. The computed maximum total gain is 1.31 dB. Figure 6b demonstrates cross polarization (*Gy*). The antenna is linearly polarized with a low cross–polarization as we would expect from a small loop antenna.

5. CONCLUSION

The ECLA was introduced as a magnetic field antenna (electric current). This antenna was designed as a dual for the PIFA. The ECLA was simulated using HFSS to compute its return loss and far–field pattern. The computed return loss had a good agreement with the simulation results. This antenna can be used in applications with low electric field intensity in the near zone such implanted antennas.

REFERENCES

1. M. A. Jensen and Y. Rahmat-Samii, EM interaction of handset antennas and a human in personal communications, Proc IEEE 83 (1995), 7–17.
2. J.F. Deford, O.P. Gandhi, and M.J. Hagmann, Moment-method solutions and SAR calculations for inhomogeneous models of man with large number of cells, IEEE Trans Microwave Theory Tech 31 (1983), 848–851.
3. R.F. Harrington, Time-harmonic electromagnetic fields, McGraw-Hill, New York, 1961.
4. T. Taga and K. Tsunekawa, Performance Analysis of a Built-In Planar Inverted F Antenna for 800 MHz Band Portable Radio Units, IEEE J Selected Areas Commun 5 (1987), 921–929.
5. K. Kobayashi, S. Nishiki, T. Taga, and A. Sasaki, Detachable mobile radio units for the 800 MHz land mobile radio system, 34th IEEE Vehicular Technology Conference, 1984, pp. 6–11.
6. M. Manteghi and Y. Rahmat-Samii, A novel miniaturized triband PIFA for MIMO applications, Microwave Optl Technol Lett 49 (2007), 724–731X.
7. L.J. Chu, Physical limitations of omni-directional antennas, J Appl Phys 19 (1948), 1163–1175.
8. M.C. Huynh and W. Stutzman, Ground plane effects on planar inverted-F antenna (PIFA) performance, IEEE Proc Microwaves Antennas Propag 150 (2003), 209–213.

BIDIRECTIONAL RECTANGULAR RING ANTENNA FOR COAL MINE/TUNNEL COMMUNICATION

Wendong Liu, Zhijun Zhang, and Zhenghe Feng
State Key Laboratory of Microwave and Communications, Department of Electronic Engineering, Tsinghua University, Beijing 100084, China; Corresponding author: zjzh@tsinghua.edu.cn

Received 20 September 2012

ABSTRACT: *A bidirectional antenna, which is useful in coal mine or tunnel wireless communication, is proposed in this article. The antenna consists of a probe excited rectangular ring. The dimensions of the rectangular ring are 147 × 20 × 40 mm³ (0.45λ × 0.06λ × 0.12λ). The length of the feeding probe is 15 mm (0.045λ). The measured −10 dB bandwidth is ∼14 MHz (910–924 MHz), and the corresponding peak gain is 5.8 dBi. Radiation patterns are measured and compared to the simulation results. The proposed bidirectional antenna has the advantages of low cost, low-profile, easy fabrication, small cross-section to the ventilation direction, and good bidirectional radiation.* © 2013 Wiley Periodicals, Inc. Microwave Opt Technol Lett 55:1412–1416, 2013; View this article online at wileyonlinelibrary.com. DOI 10.1002/mop.27552

Key words: *bidirectional antenna; coal mine communication; tunnel communication*

1. INTRODUCTION

Electromagnetic waves suffer from high path loss and multipath attenuation in mines or tunnels and do not propagate well [1]. In such long and narrow service area, the bidirectional high gain antenna alleviates the path loss and extends the coverage of relay stations of a booster system. Traditionally, bidirectional antennas are made by combining two unidirectional antennas such as Yagi-Uda [2]. In Ref. 3, a four-element coplanar waveguide fed back-to-back patch antenna array was set to achieve a bidirectional radiation pattern. Antennas with low profile are needed, because many tunnels in coal mines are so narrow that only one man can pass through. However, such schemes in Refs. 2 and 3 are difficult to miniaturize the dimension due to the complicated feed network and power loss. Slot antenna etched on a finite ground has a bidirectional radiation pattern, and the max gain is usually around 5 dBi [4]. In most mines, hazardous gases such as methane and carbon monoxide leak spontaneously, which may cause explosions or suffocation. So ventilation with wind velocity of 2–6 m/s must be guaranteed to maintain a safe level of oxygen (19.5–23.5% by volume) and reduce the content of other harmful gases. The broadside bidirectional planar antennas [3, 4] with a large cross-section size would hinder the ventilation in a narrow mine tunnel and thus are not suitable for application in mines. In Ref. 5, a notch antenna cut in a sheet conductor was proposed for bidirectional radiation. However, when installed on a small mounting board, the radiation pattern is tilted up from the board. By adding parasitic elements, the pattern is tilted downward efficiently [6]. For coal mine communication, coal dust accumulating on such large surface of the antennas [5, 6] would degrade their radiation performance gradually and severely. Spiral antenna [7] is known as a wideband circularly polarized bidirectional antenna. However, the max gain is low (around 2 dBi). A bidirectional narrow patch antenna with narrow patches of the same size on both sides of a thin substrate (0.02λ) was presented in Ref. 8, which also suffers from low gain (about −2 dBi), and parasitic elements are needed to improve the gain. Besides, cost effectiveness must be taken into consideration for the number of the relay stations is large. A simple and cost-effective bidirectional antenna using a monopole in a rectangular waveguide was reported in Ref. 9.

For the above-mentioned facts, antennas with low cost, low-profile, small cross-section, and good bidirectional radiation are highly desirable for communications in mines. Therefore, a rectangular loop antenna excited by a linear probe is proposed to meet such demands. Compared to the design in Ref. 9, the geometrical structure appears similar, but the work principle is different. In Ref. 9, the radiation is attributed to the monopole, and the waveguide operating in transverse electric $(TE)_{10}$ mode is used to confine the radiation pattern. In this article, the rectangular ring works in a 1λ loop mode, and the radiation is attributed to the in-phase currents on the two short edges of the ring. The short probe does not participate in radiation but only works for impedance matching. Thus, a lower profile can be achieved compared to the design in Ref. 9. The dimensions of the

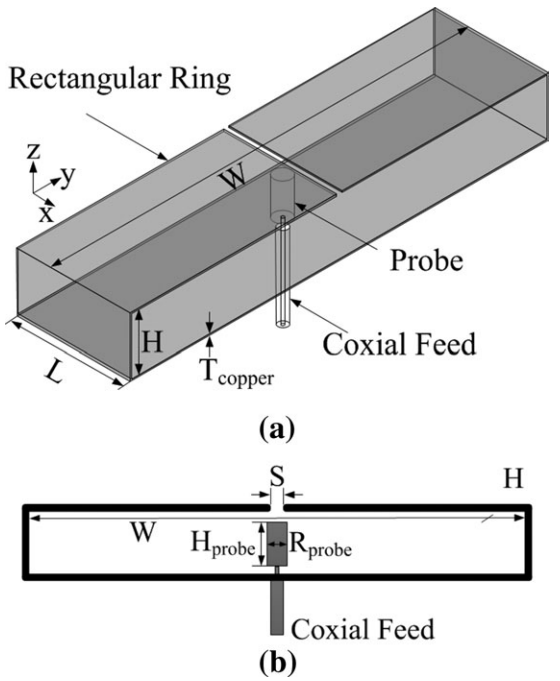

Figure 1 Geometry of the proposed antenna: (a) 3D view and (b) cross-section

rectangular ring are 147 × 20 × 40 mm^3 (about 0.45λ × 0.06λ × 0.12λ, where λ corresponds to 915 MHz). The length of the probe is 15 mm (0.045λ).

2. ANTENNA DESIGN

The geometry of the proposed bidirectional antenna is shown in Figure 1. A rectangular copper ring of width $W = 147$ mm, height $H = 20$ mm, and length $L = 40$ mm is used. The thickness of the copper is 0.4 mm. The radius of the short linear probe is 3 mm, and the height is 12 mm. A coaxial cable is used to feed the probe with the inner conductor connected to the probe and the outer conductor connected to the rectangular ring. As shown in Figure 1, the inner conductor extends into the rectangular ring for 2 mm; thus, the total length of the probe is 15 mm. Detailed parameters are provided in Table 1.

2.1. Bidirectional Radiation of the Rectangular Ring

The proposed antenna originates from the traditional square loop shown in Figure 2(a). The modified loop in Figure 2(b) is transformed from the square loop, which is the prototype of the proposed design. The perimeters of the two loops are almost the same 1λ. The feeding method is changed for impedance matching. Figure 3 shows the simulated radiation patterns of the loops in E plane. The simulated max directivity of rectangular loop is 5.5 dBi, which is 2 dB higher than that of the square one. The main radiation of the two loops mainly comes from the two edges with currents in phase as shown in Figure 2. The two radiation edges can be treated as a two-element array. As the distance between the two elements increases from about $\lambda/4$ to $\lambda/2$, the cancellation in y direction increases, and, therefore, the radiation in z direction

TABLE 1 Dimensions of the Proposed Antenna

Parameters (mm)						
W	H	L	T_{copper}	H_{probe}	R_{probe}	S
147	20	40	0.4	1	3	2

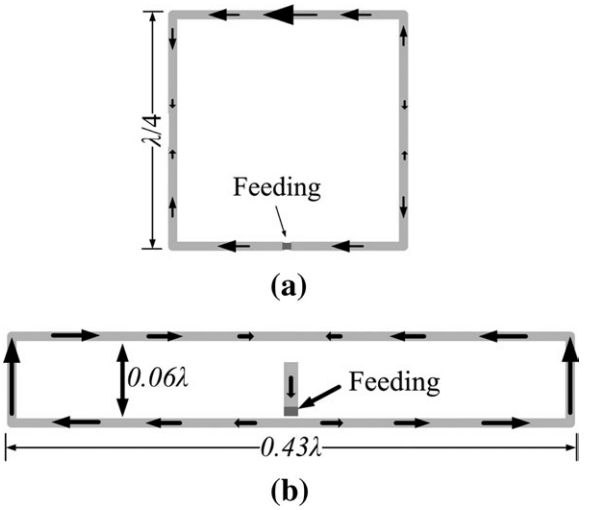

Figure 2 Current distributions: (a) traditional loop and (b) rectangular loop similar to the proposed antenna

increases. The proposed antenna works in the same way as the loop shown in Figure 2(b), which can be verified from the current distribution shown in Figure 4. The rectangular ring is the main radiator, and it is not working as a rectangular waveguide, because the width of the rectangular ring is about 0.45λ, and the basic TE_{10} mode cannot propagate, which is different from that in Ref. 9. Compared to the current on the two vertical edges, the current of the probe is quite weak and in opposite phase. It is not a radiation part but only works for impedance matching. On the other hand, the probe in Ref. 9 works as a monopole, and the current on the probe is the strongest. The main radiation comes from the monopole, and its radiation pattern is confined by the rectangular waveguide providing bidirectional beam in the forward and backward directions along the ring aperture.

2.2. Impedance Matching

The effect of the key geometrical parameters on the antenna impedance matching has been studied. The other parameters were

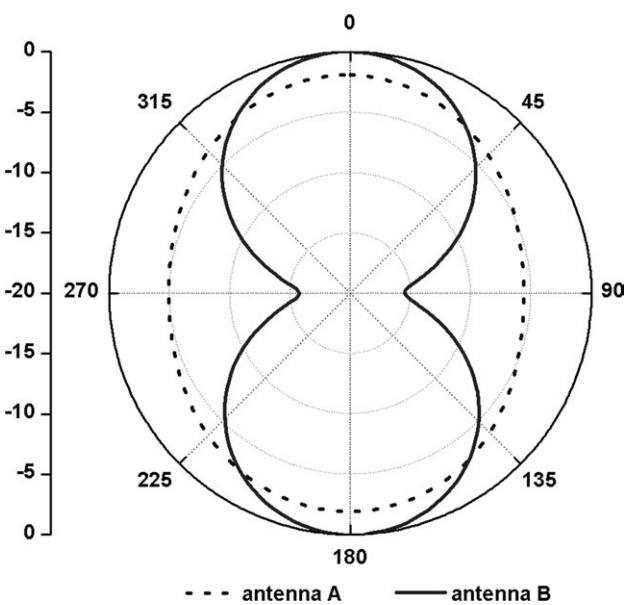

Figure 3 Radiation pattern comparisons in E plane between the traditional loop and rectangular loop similar to the proposed antenna

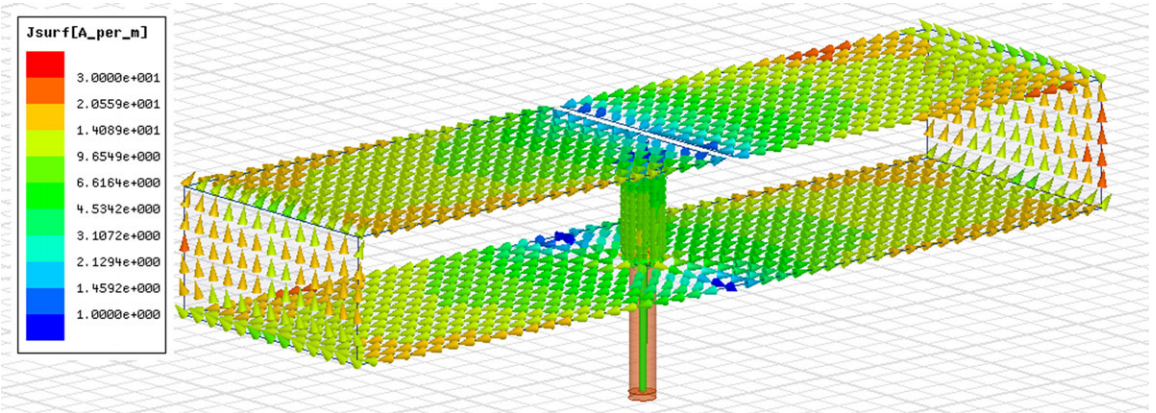

Figure 4 Current distribution of the proposed antenna. [Color figure can be viewed in the online issue, which is available at wileyonlinelibrary.com]

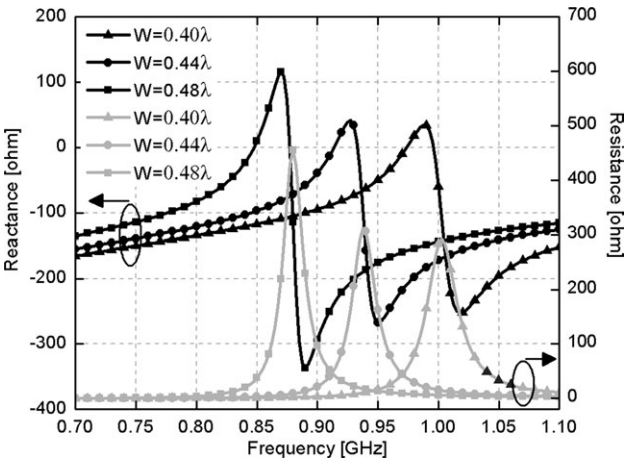

Figure 5 Simulated input impedance varying with parameter W

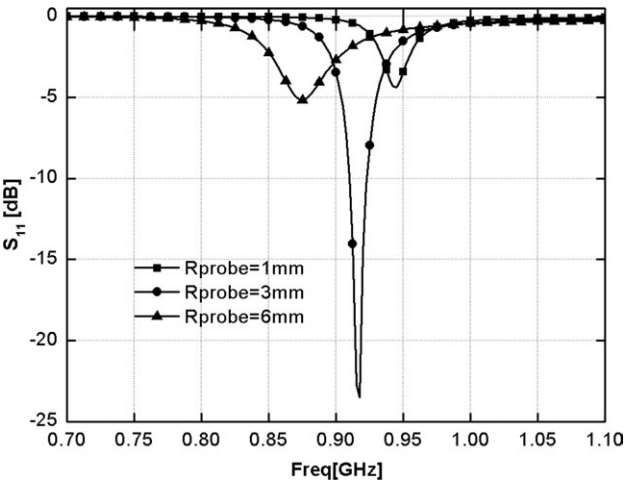

Figure 7 Simulated reflection coefficients varying with parameter R_{probe}

kept unchanged as the values in Table 1, when the influence of a particular parameter was investigated. The simulation software high frequency structure synthesizer (HFSS) was used in the study.

The input impedance of the antenna for different rectangular ring widths is illustrated in Figure 5. The variation of the width W of the rectangular ring changes the resonant frequency. As analyzed previously, the resonant loop mode is decided by the perimeter of the rectangular ring, and the simulated results verify the conclusion. The parameter W decides the distance of the two in-phase vertical currents of the ring. For a given ring perimeter, the directivity of the ring will get higher, as W gets larger. Meanwhile, the distance between the horizontal currents out of phase gets closer and the cancellation gets stronger, which leads to a higher Q value and narrower bandwidth of the antenna. In the design, there is a tradeoff between the directivity and the bandwidth. In the design, it is the rectangular ring with a certain length L that is selected, not the original rectangular loop. One concern is to ensure that the whole structure is solid enough for application in underground mines. Another reason is to tune the impedance matching. Figure 6 shows the reflection coefficient for different length L of the rectangular ring. As L

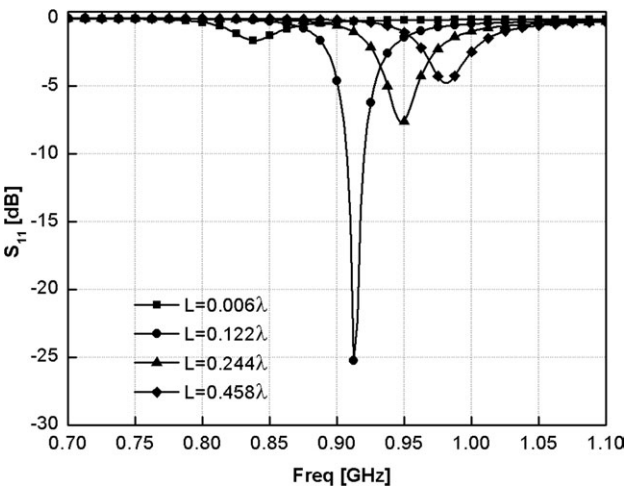

Figure 6 Simulated reflection coefficients varying with parameter L

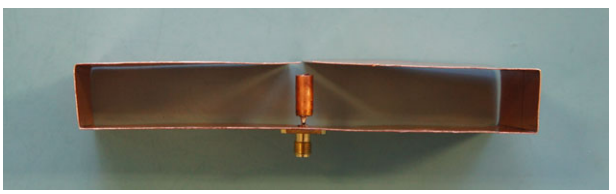

Figure 8 Photograph of the proposed antenna. [Color figure can be viewed in the online issue, which is available at wileyonlinelibrary.com]

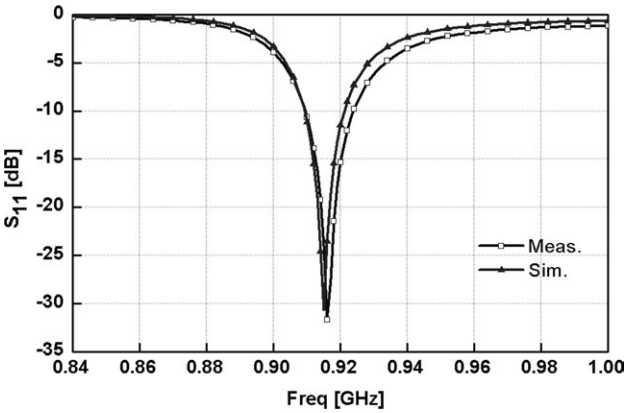

Figure 9 Simulated and measured reflection coefficients of the proposed antenna

decreases to 1 mm, the antenna becomes a real loop. While L gets larger, the rectangular ring will behave as a rectangular waveguide. Due to the special dimension, no propagation mode can exist, which makes the impedance matching almost impossible. So a quasiloop structure shows its advantage in impedance matching. Another important factor in the impedance matching is the radius of the feed probe. As shown in Figure 7, by adjusting R_{probe}, the input impedance of the antenna can be matched to 50 Ω.

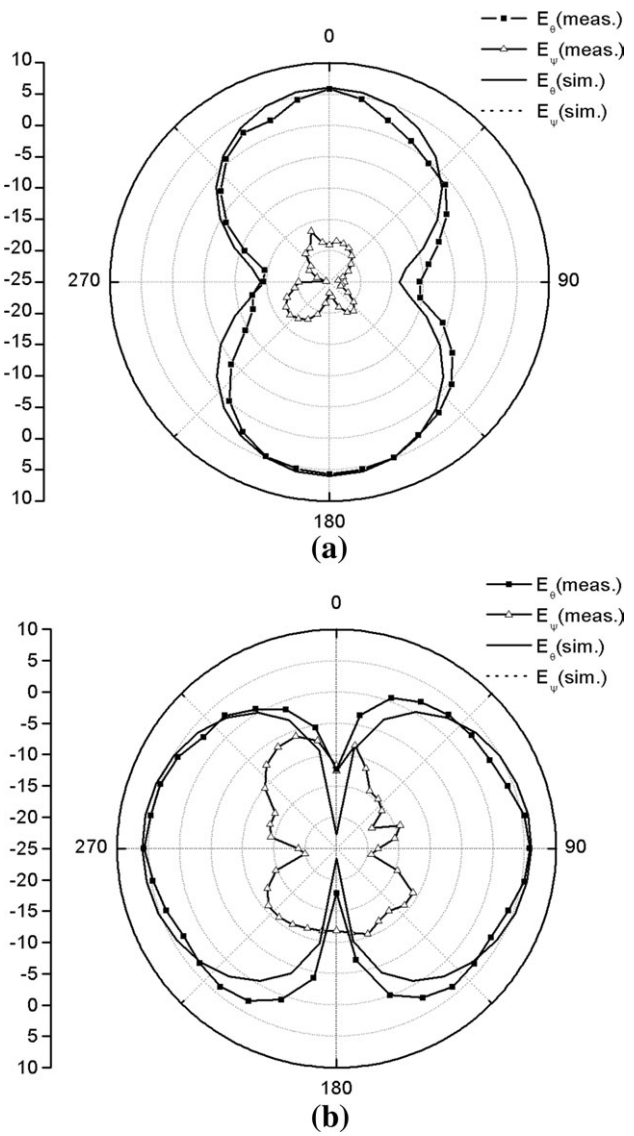

Figure 10 Simulated and measured radiation pattern of the proposed antenna: (a) H plane (xy plane) and (b) E plane (xz plane)

3. RESULTS AND DISCUSSION

According to the parameters given in Table 1, a prototype was fabricated by folding a copper sheet symmetrically, as shown in Figure 8. Thus, the rectangular ring is not closed, and the gap is characterized by the parameter S. According to the electric current distribution in Figure 2(b), the gap is just located at the place where the current is zero; thus, little influence on the current distribution is induced. Because a coaxial cable is attached to the prototype as an excitation in the measurement, a $\lambda/4$ balun is used to reduce the surface current along the coaxial cable. The measured results were performed by a vector network analyzer (Agilent ENA E5071B). The radiation patterns were measured in a standard anechoic chamber. Both the simulated and the measured reflection coefficients are shown in Figure 9, the simulated center frequency is 915 MHz, the −10 dB impedance bandwidth is about 12 MHz (909–921 MHz), the measured center frequency is 915.5 MHz, and the −10 dB impedance bandwidth is 14 MHz (910–924 MHz). Differences between the simulated and measured results are mainly caused by the fabrication tolerance and loss. The simulated and the measured normalized radiation patterns at 915 MHz in the x–y and x–z planes are shown in Figure 10, which show good consistency. Bidirectional radiation patterns are obtained. The simulated peak gain of the proposed antenna is 6 dBi at 915 MHz, while the measured gain is 5.8 dBi.

5. CONCLUSION

This article presented a bidirectional antenna using a linear probe excited rectangular ring. The working principle of the proposed antenna is discussed. The proposed bidirectional antenna inherits the merits of low cost, easy fabrication, small cross-section size, and low profile, which is quite suitable for wireless communication in coal mines. The measurement results agree well with simulation data and illustrate excellent bidirectional radiation character.

ACKNOWLEDGMENTS

This work is supported by the National Basic Research Program of China under Contract 2010CB327402, in part by the National High Technology Research and Development Program of China (863 Program) under Contract 2011AA010202, the National Natural Science Foundation of China under Contract 60771009, the National Science and Technology Major Project of the Ministry of Science and Technology of China 2010ZX03007-001-01, and Qualcomm, Inc.

REFERENCES

1. P. Delogne, EM propagation in tunnels, IEEE Trans Antennas Propag 39 (1991), 401–406.
2. J.D. Kraus, Antennas, Chapter 8, McGraw-Hill, New York.
3. H. Iwasaki, Microstrip antenna with back-to-back configuration relative to a slot on a ground plane, Electron Lett 34 (1998), 1373–1374.
4. Y. Li, Z. Zhang, W. Chen, Z. Feng, and M.F. Iskander, A dual-polarization slot antenna using a compact CPW feeding structure, IEEE Antennas Wireless Propag Lett 9 (2010), 191–194.

5. H. Arai and K. Kohzu, A bidirectional notch antenna, In: IEEE Antennas and Propagation Society International Symposium, Vol. 1, Baltimore, MD, 1996, pp. 42–45.
6. H. Arai, K. Kohzu, and T. Mukaiyama, Bi-directional notch antenna with parasitic elements for tunnel booster system, In: IEEE Antennas and Propagation Society International Symposium, Vol. 4, Montreal, Canada, 1997, pp. 2218–2221.
7. J.D. Dyson, The equiangular spiral antenna, IRE Trans Antennas Propag 7 (1959), 181–187.
8. K. Cho and T. Hori, Bidirectional rod antenna composed of narrow patches, In: IEEE Antennas and Propagation Society International Symposium, Vol. 1, Seattle, WA, 1994, 174–177.
9. C. Phongcharoenpanich, T. Sroysuwan, P. Wounchum, S. Kosulvit, and M. Krairiksh, Theory and experiment of an antenna using a probe excited rectangular ring, In: IEEE Antennas and Propagation Society International Symposium, Columbus, OH, Vol. 3, 2003, 737–740.

EFFECTIVE DIELECTRIC CONSTANT OF TOP GROUNDED COPLANAR WAVEGUIDE ON LIQUID CRYSTAL SUPERSTRATE

Senad Bulja,[1] Dariush Mirshekar-Syahkal,[2] Richard James,[3] Sally E. Day,[3] and F. Aníbal Fernández[3]
[1] Bell Labs Ireland, Blanchardstown Industrial Park, Dublin 15, Ireland
[2] School of Computer Science and Electronic Engineering, University of Essex, Colchester CO4 3SQ, United Kingdom
[3] Department of Electronic and Electrical Engineering, University College London, Torrington Place, London WC1E 7JE, United Kingdom; Corresponding author: senad.bulja@alcatel-lucent.com

Received 26 September 2012

ABSTRACT: *The effective dielectric constant of the top grounded coplanar waveguide with a liquid crystal (LC) superstrate for phase shifting applications is investigated in the frequency range of 30–60 GHz. Two nematic LC mixtures, namely E7 and MDA-00-3506, are used as the superstrate. The measurements show that MDA-00-3506 offers higher values of phase shift per millimeter than its E7 counterpart. In particular, the MDA-00-3506 provides 3.14°/mm, whereas E7 gives 2.79°/mm at 60 GHz. The results of the dielectric constants from measurement and computer modeling are found to agree to within 5%. For the modeling, a comprehensive finite element package predicting the local alignment of LC molecules and effective dielectric constant at different bias voltages and frequencies are used.* © 2013 Wiley Periodicals, Inc. Microwave Opt Technol Lett 55:1416–1418, 2013; View this article online at wileyonlinelibrary.com. DOI 10.1002/mop.27564

Key words: *CPW; liquid crystal; finite element method; mm-wave devices*

1. INTRODUCTION

The abundance of a widely available spectrum between 30 and 60 GHz (in mm-wave region) offers potential for the development of high data rate, short-range wireless communications [1].

Nematic liquid crystals (LCs) are relatively cheap and their dielectric constants, which have a tensor form, can be controlled by an external electric or magnetic field. This property of nematic LCs has already been exploited for the development of tunable antennas [2] and phase shifters [3].

The choice of a suitable LC for a particular mm-wave application depends on many factors, however, by far the most influential one is the dielectric anisotropy, $\Delta\varepsilon = \varepsilon_{\parallel} - \varepsilon_{\perp}$, as it directly influences the tunability of an LC-based device.

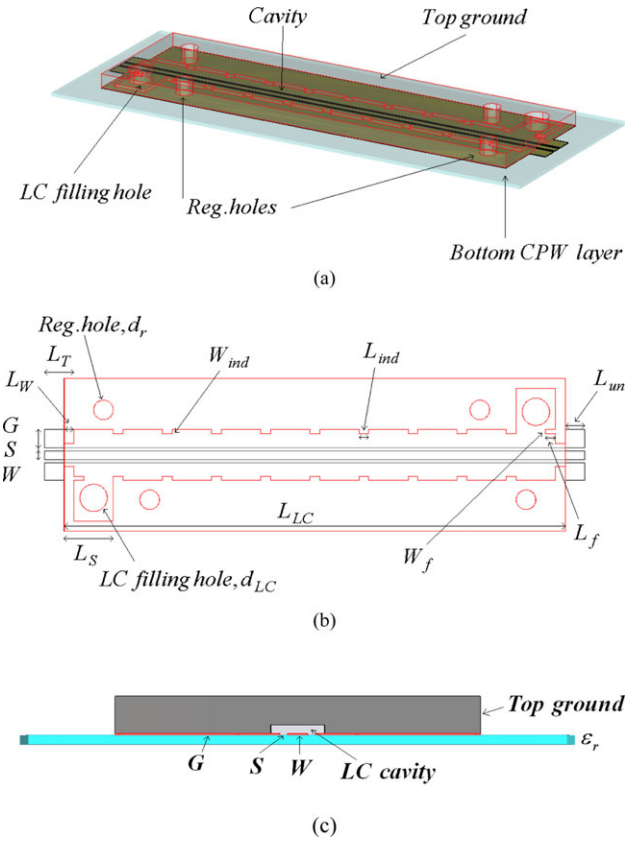

Figure 1 Device structure for measurement of effective dielectric constant of top grounded CPW with LC superstrate: (a) perspective, (b) top, and (c) cross-section views (not to scale). [Color figure can be viewed in the online issue, which is available at wileyonlinelibrary.com]

LC-based mm-wave devices can be developed using various planar transmission lines including the microstrip line and coplanar waveguide (CPW). However, the implementation of an LC layer as a substrate in a microstrip line and integrating this line with the rest of microstrip lines in a circuit are difficult, while an LC superstrate can be realized in a part of a CPW circuit with relative ease.

In this article, the variation of the effective dielectric constant of the top grounded CPW loaded with an LC superstrate with frequency and LC bias voltage is investigated, and its use in phase shifting applications is outlined. The frequency range considered is 30–60 GHz. In the investigation, two different LCs, known as E7 and MDA-00-3506, are used. The measured effective dielectric constants are then compared with those obtained from a finite element modeling developed by the authors for the analysis and design of LC-based planar structures [4].

2. MEASUREMENT DEVICE AND TECHNIQUE

The top grounded CPW with the LC cell as its superstrate is shown in Figure 1. For the dielectric characterization purpose, a length of the top grounded CPW with the LC cell (superstrate) is terminated into two short sections of ungrounded CPWs. In fact, the use of CPW electrodes allows for the measurements of *S*-parameters using a probe station at different bias voltages supplied through a wideband bias tee. The rotation of the LC molecules in the LC cell is achieved by applying low frequency and low voltage across the electrodes of the ungrounded CPW [4], which is in contrast to the magnetic field biasing method used in Ref. 5.